Available online at www.sciencedirect.com
ScienceDirect
Journal of Hydrodynamics
2014,26(6):930-938
DOI: 10.1016/S1001-6058(14)60102-5
www.sciencedirect.com/science/journal/l0016058

Numerical computations of resistance of high speed catamaran in calm water*

ZHA Ruo-si (查若思), YE Hai-xuan (叶海轩), SHEN Zhi-rong (沈志荣), WAN De-cheng (万德成)
State Key Laboratory of Ocean Engineering, School of Naval Architecture, Ocean and Civil Engineering, Shanghai Jiao Tong University, Shanghai 200240, China, E-mail: zharuosi@163.com

(Received February 7, 2014, Revised September 9, 2014)

Abstract: In this paper, the in-house multifunction solver naoe-FOAM-SJTU is applied to study the resistance and wave-making performance of a high-speed catamaran sailing at different velocity in calm water. The volume of fluid (VOF) method is used to capture the free interface and the finite volume method (FVM) is adopted as the discretization scheme. The hull model is fixed with initial trim and sinkage. The numerical results of the presented paper agree very well with the measurement data of model test. Wave making and vortex field are well simulated to analyze the hydrodynamic performance of a catamaran.

Key words: OpenFOAM, viscous flow, resistance, wave-making, naoe-FOAM-SJTU solver

Introduction

For several decades, the application of multi-hull ship has made a rapid progress in both civil and military fields. As one of the high performance ships, catamaran which has two symmetry hulls is expected to be further developed owing to its excellent performances concerning the resistance, stability and maneuverability.

A study of the catamaran resistance performance in calm water is conducted in this paper. The traditional research methods include a variety of experimental model tests, experience formulas and numerical simulations. The method of computational fluid dynamic (CFD) has been increasingly developed to solve the hydrodynamic problems in recent years. The viscous effects of fluid can be fully taken into consideration and non-linear factors can be handled precisely, especially in the conditions of high Reynolds number. With the advancements of computer science and mature numerical computation methods, nowadays the efficiency and accuracy of CFD method are greatly improved. As a consequence, the combination of model test and CFD method is becoming an optimum choice to study the catamaran issues.

Sahoo et al.[1] used Shipflow to compute the wave-making resistance of a staggered catamaran based on the CFD method. Chen et al.[2] used the modified Dawson method to develop a numerical prediction program for the resistance calculation of catamaran and trimaran. Castiglione et al.[3] used CFDSHIP-Iowa to study the seakeeping behavior of the DELFT catamaran model by the unsteady RANS method. Their results were compared with those obtained with VERES by Carrica et al.[4]. Deng et al.[5] discussed the influencing factors and numerical schemes of hydrodynamic calculation using Fluent. Jamaluddin et al.[6] adopted both model test and numerical computation to analyze the resistance component interactions of specified catamarans.

In this paper, a CFD method was applied to simulate the viscous flow field and compute the resistances of a typical catamaran form. Compared with using commercial software directly, the solver by independent development based on open source code package is more flexible and extensible for multi-aspect issues. Based on OpenFOAM[7], the in-house solver naoe-FOAM-SJTU[8] is appropriate for various kinds of complex hydrodynamic issues of naval architecture and ocean engineering. Previous works have made many progresses in developing and validating

* Project supported by the National Natural Science Foundation of China (Grant Nos. 11072154, 51379125), the National Key Basic Research Development Program of China (973 Program, Grant No. 2013CB036103).
Biography: ZHA Ruo-si (1992-), Male, Master Candidate
Corresponding author: WAN De-cheng,
E-mail: dcwan@sjtu.edu.cn

this solver applied in this paper. In 2011, Cha and Wan[9] firstly accomplished the numerical wave generation and absorption. Shen and Wan[10] simulated the viscous flow acting on KVLCC2, KCS, and DTMB5415 and compared with the measurement results by naoe-FOAM-SJTU. Ye and Wan[11] computed the added resistance in regular head waves with ship trim and sinkage, and validated the ability of naoe-FOAM-SJTU to solve the strongly nonlinear problems. Cao and Wan[12] studied the extreme wave effects on cylindrical offshore structures by naoe-FOAM-SJTU. Liu and Wan[13] used naoe-FOAM-SJTU to simulate motion responses of an offshore observation platform in regular waves.

1. Numerical methods

1.1 *Governing equations*

In the simulation of unsteady incompressible viscous two-phase flow field, the Reynolds-averaged Navier-Stokes (RANS) equations are applied in this paper as governing equations. The equation of continuity and momentum equation can be written as

$$\nabla \cdot \boldsymbol{U} = 0 \tag{1}$$

$$\frac{\partial \rho \boldsymbol{U}}{\partial t} + \nabla \cdot [\rho(\boldsymbol{U} - \boldsymbol{U}_g)\boldsymbol{U}] = -\nabla p_d - \boldsymbol{g} \cdot x \nabla \rho + \nabla \cdot (\mu_{eff} \nabla \boldsymbol{U}) + (\nabla \boldsymbol{U}) \cdot \nabla \mu_{eff} + f_\sigma + f_s \tag{2}$$

in which $\boldsymbol{U}$ stands for the velocity field while $\boldsymbol{U}_g$ means velocity of mesh points, p_d is dynamic pressure, whose value is equal to total pressure subtracting hydrostatic component, ρ is mixed density of the two phases, $\boldsymbol{g}$ is the gravitational acceleration, μ_{eff} is the effective dynamic viscosity computed by $\rho(\nu + \nu_t)$, where ν is kinematic viscosity coefficient and ν_t is eddy viscosity, f_σ is a surface tension term, which impacts the free surface. To protect the flow field from the interference of echo waves, the source term f_s is added to generate a sponge layer to absorb the generated wave[14].

The SST k-ω model[15] is applied as the turbulence model in this paper. This turbulence model synthesizes the advantages of standard k-ω model and k-ε model. The former one is appropriate to simulate the turbulent flow far way the wall plane, while the latter is good at handling the boundary flow near the wall under different pressure gradients. The accuracy of numerical computation is satisfactory by using the SST k-ω turbulence model.

1.2 *Capture of free surface*

In naoe-FOAM-SJTU, two methods are available to simulate the free surface of the two-phase flow, including the volume of fluid (VOF) and level-set method. The VOF method with artificial bounded compression technique[16] is used for simulating free surface in this paper. The VOF transport equation is formulated as follows:

$$\frac{\partial \alpha}{\partial t} + \nabla \cdot [(\boldsymbol{U} - \boldsymbol{U}_g)\alpha] + \nabla \cdot [\boldsymbol{U}_r(1-\alpha)\alpha] = 0 \tag{3}$$

where α represents the volume of fraction, the relative proportion of the two phase fluid, α is used to distinguish the fluid of two phases, defined as

$$\alpha = 0 \quad \text{air} \tag{4a}$$

$$\alpha = 1 \quad \text{water} \tag{4b}$$

$$0 < \alpha < 1 \quad \text{interface} \tag{4c}$$

The fluid density ρ and dynamic viscosity μ are obtained by

$$\rho = \alpha \rho_t + (1-\alpha)\rho_g \tag{5}$$

$$\mu = \alpha \mu_t + (1-\alpha)\mu_g \tag{6}$$

where the subscript l and g refer to liquid and gas respectively. The surface tension in Eq.(2) is defined as

$$f_\sigma = \sigma \kappa \nabla \alpha \tag{7}$$

where σ is the surface tension. Its value is set as 0.07 kg/s^2 in this paper, κ is the curvature of surface interface

$$\kappa = -\nabla \cdot n = -\frac{\sum_f S_f \cdot n_f}{V_i} \tag{8}$$

V_i is volume of cell, the subscript f means that the value is computed at cell face, $\sum_f S_f$ represents the sum magnitude of face area where S_f is normal vector of cell face, the unit normal vector on interface n_f is given as

$$n_f = \frac{(\nabla \alpha)_f}{\left|(\nabla \alpha)_f + \delta\right|} \tag{9}$$

where δ is the stabilization factor defined as

Table 1 Main dimensions and particulars

Main Features	Symbol	Full scale	Model
Scale ratio	λ	1	20
Length between perpendiculars	L_{pp} (m)	54.200	2.710
Length of waterline	L_{wl} (m)	54.200	2.710
Breadth	B (m)	16.720	0.836
Draught	T (m)	2.830	0.142
Displacement	Δ (kg)	550000	68.750
Demi-hulls separation	S_c (m)	13	0.650
Wetted surface	S (m^2)	762.200	1.906
Longitudinal center of gravity	LCG (m)	30.880	1.544
Vertical center of gravity	KG (m)	5.600	0.280
Longitudinal inertia radius	K_{yy} (m)	14.634	0.732
Transverse inertia radius	K_{xx} (m)	5.852	0.293
Longitudinal inertia moment	I_{yy} ($kg\cdot m^2$)	1.1778×10^8	36.808
Transverse inertia moment	I_{xx} ($kg\cdot m^2$)	1.8835×10^7	5.886

$$\delta = \frac{1\times10^{-8}}{\left(\dfrac{\sum_{i=1}^{N} V_i}{N}\right)^{1/3}} \tag{10}$$

in which N stands for total cells amount of the mesh.

Moreover, the first two terms on the left hand side of Eq.(3) stand for traditional VOF transport equation and the other term represents the artificial compression term. The appearance of the term $(1-\alpha)\alpha$ makes the compression term take effect only on the interface without affecting the numerical computation out of the transition layer. U_r is the velocity field for compressing the interface. The velocity field can be computed at cell faces by the maximum velocity magnitude at the interface region, defined as

$$U_{r,f} = n_f \min\left\{C_\alpha \frac{|\phi|}{S_f}, \max\left(\frac{|\phi|}{S_f}\right)\right\} \tag{11}$$

where φ is face volume flux, including the flux of grid velocities from the PISO algorithm, C_a is a compression coefficient indicating the degree of compression. It is set as 1 in this paper based on previous experience.

1.3 *Discretization of equations*

The finite volume method (FVM)[17] is used to discretize both the RANS equations and VOF transport equation in naoe-FOAM-SJTU. According to FVM, the computational domain is partitioned into grid cells and each grid node is surrounded by a control volume. Field information is stored at the center of cells. Then cell center values are interpolated into face values, which are summed to compute the volume integration. Different interpolation schemes are applied. In detail, a second-order TVD limited linear scheme is used to discretize the convection terms in Eq.(2), the diffusion terms are discretized by a second-order central difference scheme, the Van Leer scheme is applied for VOF equation discretization, a second-order backward method is applied for temporal discretization.

For the discretized RANS equations, the pressure-implicit-split-operator (PISO) algorithm[18] is adopted to solve the coupled equation of velocity and pressure. Each PISO loop contains three steps, namely prediction, correction and second correction. The second correction can make velocity and pressure correspond with the momentum equation and continuity equation more effectively so that the convergence of each loop is accelerated.

2. Ship model and case conditions

2.1 *Hull model*

A high-speed catamaran in model scale is studied in this paper. The main dimensions and particulars are listed in Table 1, including both the full scale and the model scale. The 3-D models of twin hulls are shown in Fig.1, including the bow, stern and overall hull. In order to obtain a mesh with good quality, the sides of hull deck and stern plate are rounded off.

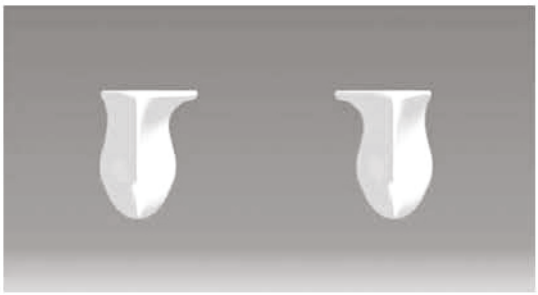

(a) Transverse of two hulls

(b) Stern shape

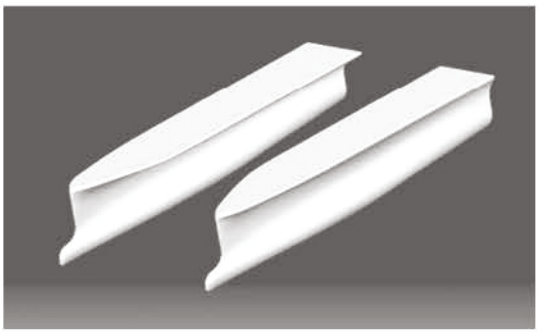

(c) Overall view

Fig.1 The 3-D models of the catamaran

2.2 *Case conditions*

To compare the numerical simulation with model test, the case conditions are set identically to the test conditions. The ambient temperature of the model test is 14.2°C. The water density is 999.415 kg/m^3 and the kinematic viscosity is 1.163×10^{-6} m^2/s. The value of gravitational acceleration is 9.81 m/s^2.

In this paper, three cases of different ship velocities are simulated. At the beginning of each simulation, hulls are not under upright condition but sailing with a certain trim angle and sinkage according to the model test. The six degree-of-freedoms of hulls are fully fixed during the following computation. The Froude number of the model hull of each case is shown in Table 2, along with the initial trim angle and sinkage of each case. The origin of the earth coordinate system is located at the intersection of water plane. In terms of the trim angle, positive value means trim by bow, and negative value means trim by stern.

Table 2 Main dimensions and particulars

V (m/s)	Fr	Trim (°)	Sinkage (10^{-2}m)
1.0	0.194	0.077	–0.246
2.0	0.388	0.186	–1.291
4.0	0.776	–1.230	–3.413

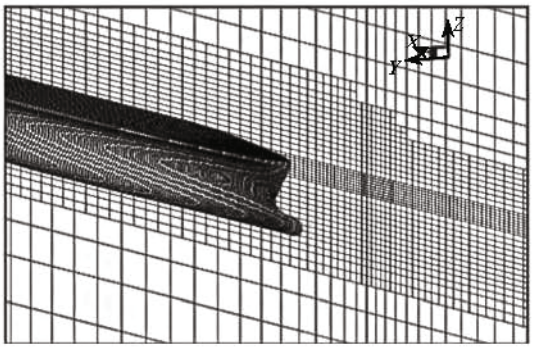

(a) Grid near the bow

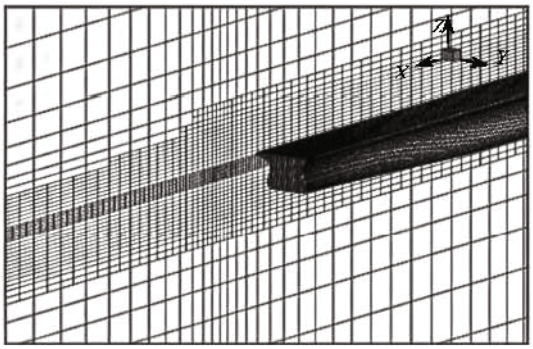

(b) Grid near the stern

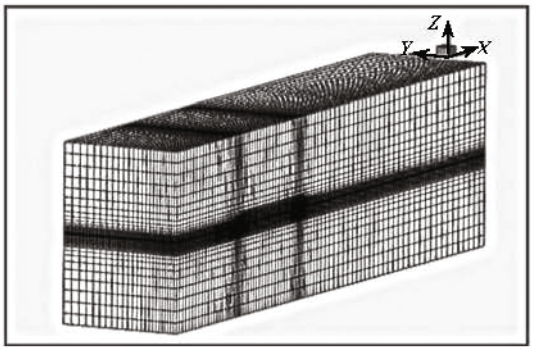

(c) Overall domain mesh

Fig.2 Mesh generation

3. Mesh and domain

A half of whole flow field with only one hull is adopted owing to the symmetry of problem. The total force of twin hulls is as twice as the result of one hull. The computation results have contained the drag addition from the wave disturbance between the two hulls due to the use of symmetry boundary condition.

For the three cases in this paper, a same computing domain is used to simulate the flow field around the hull. The space coordinate range is determined as $-1.0L_{pp} < x < 4.0L_{pp}$, $0 < y < 1.0L_{pp}$, $-1.0L_{pp} < z < 1.0L_{pp}$. The mesh is generated by SnappyHexMesh, the mesh generation utility of OpenFOAM.

The overall domain mesh and the details near the bow and stern are displayed in Fig.2. The grids of important regions are refined to capture precisely the free surface and the wake flow field, and accurately compute the variables near wall region of the hull. The refinement domains consist of the boundary layer around the hull, the interface region, the area near bulbous bow and the rear of stern. Near 10^6 cells for a case are generated. The cell amounts of three cases in this paper are not identical, resulting from the different configuration. With high Froude number, the variables in a small region of the flow field change heavily. For the case of high speed, the refinement regions are expanded and the refinement levels are improved to keep an acceptable accuracy.

Table 3 Numerical results for model scale catamaran

Fr	F_p (kg)	F_f (kg)	F_t (kg)	F_t_test (kg)	Error
0.194	0.185	0.360	0.545	0.559	2.50%
0.388	1.165	1.194	2.360	2.517	6.24%
0.776	3.685	5.163	8.849	8.351	5.96%

Note: F_f is the friction resistance caused by viscosity, F_p is the pressure resistance, F_t means the total drag force, which is the sum of and F_t test is the total resistance measured by model test.

4. Analysis of results

By iterative computations of enough time steps, the results of drag values and corresponding drag coefficients reach convergence. For each case, the average value of the convergent data is taken as the final result. In this paper, the resistance coefficient is defined as

$$C = \frac{F}{0.5 \cdot \rho S V^2} \tag{12}$$

In Eq.(12), S is the area of wetted surface of the hull, and V is the sailing velocity. The corresponding coefficients can be calculated by Eq.(12), including C_t, C_f and C_p.

The results of all three cases are collected in Table 3, including the values of pressure drag, friction drag, total drag. The data measured by model test is provided for comparison.

The error between the numerical result and test data is calculated and shown in Table 3. For all the three conditions, the computation error of each resistance component is less than 7%, which is acceptable. As a result, the numerical simulations of this paper are reliable as a reference.

The value of resistance grows heavily with the increase of Froude number. The amplification of friction resistance is larger than that of pressure resistance. Compared with the measurement of model test, the error of high speed case is greater than that of low speed case. There are two possible reasons for this phenomenon. On one hand, the influence of nonlinear factor is amplified by the high flow velocity. On the other hand, the simulation in this paper is based on the fixed catamaran hull. The heave and pitch should not be neglected when the velocity is quite high.

The curves of comparison between the corresponding coefficients of resistance components in different velocity conditions are shown in Fig.3.

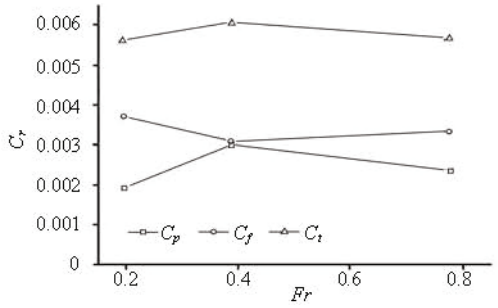

Fig.3 Comparison of resistance coefficients

The increase extent of friction resistance is smaller than the square of velocity. As a result, the friction resistance coefficient is diminishing. For 0.194 to 0.776 of the Froude number, the pressure resistance coefficient increases in a certain range and then begins to decrease, as the similar tendency of the total resistance coefficient. Thus the resistance performance of this catamaran sailing at high velocity is commendable. Limited by the number of cases in this paper, the regularity of resistance performance in the range of high speed is not clear. Further study could be carried on by simulating more cases of different velocity.

To verify and explain these regularities, a series of post-processing graphics have been displayed in the following illustrations.

4.1 *Free surface*

The wave pattern generated by the hull system in calm water is a significant factor to affect the ship resistance, especially for the wave making resistance. Meanwhile the shape of wave form can be an indicator to check whether the computation is correct. Some strongly nonlinear phenomena can be observed by the free surface. As a result, the simulation of free surface is an important aspect to study the resistance performance of this catamaran. After the steady flow field has been fully formed, the free surface of the catamaran is captured, as shown in Fig.4.

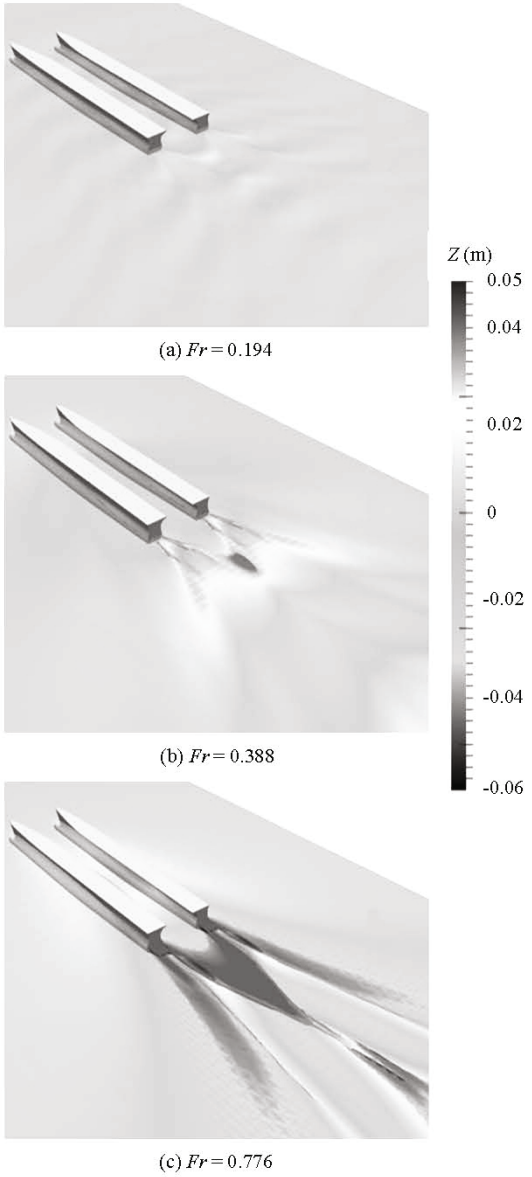

Fig.4 Free surface around the catamaran

The differences of these three cases can be analyzed by examining the steady wave making distribution around the twin hulls. Firstly, the interface near the bow of twin hulls is so flat that few of waves appear, no matter which velocity the catamaran has. Secondly, the catamaran of each case has a very different wave-making situations behind the stern. When the Froude number is 0.194, the amplitude of wave-making is relatively small. Obvious wave crest and wave trough are formed behind the stern as the Froude number increases to 0.388. The major wave crest follows the wave trough in the middle of flow field, as a result of the interference of the wave-making field between the two hulls. When the Froude number has reached 0.776, the function of interference is more apparent. Two large crests are formed immediately following the stern, which is different from the case of low and medium velocity. In addition, the wave-making region becomes small with the increase of hull velocity. The wave field in the wake flow field with low velocity is largest, while the wave-making field of higher velocity shrinks towards the symmetrical plane. For the field of high velocity, wave-making begins at aft, in front of the stern. With the increase of velocity, the major wave trough and crest move far away from the stern so that the interference shape is lankier. What is more, the stern drought of the hull decreases obviously with the increase of ship velocity. The dynamic pressure of hull stern would decrease heavily.

The extent of wave-making has a significant influence on the resistance of the catamaran. For friction, higher flow velocity leads to a larger velocity gradient in the viscosity boundary on the hull surface, which in turn gives rise to the increase of friction shearing stress. Moreover, the friction resistance of twin hulls is proportional to the wetted surface based on the hypothesis of equivalent plank. Under the condition of high velocity, the heavily changed interface results in a larger wetted surface. As a result, the friction resistance would rise with the increase of flow velocity, which is in accordance with the results of numerical simulation and model test.

The other important component is the pressure resistance, the sum of viscous pressure resistance and wave resistance. For the low velocity case, the viscous pressure resistance dominates. As the speed increases, wave resistance becomes more essential gradually. The wave-making energy is provided by the hull motion. The large value of wave resistance in the high velocity case results from the large wave amplitude and high wave velocity.

4.2 *Streamlines near the hull*

The information of the interior velocity field is used to draw the streamlines around the hull. By studying the direction and pattern of streamlines, the motion of fluid particles can be investigated and the influence of the flow field on hull can be inferred. The turbulent flow is another important factor for the increase of ship resistance. The streamlines near bow and stern of one hull under different velocity conditions are shown in Fig.5. The contour represents the ma-

gnitude of flow velocity.

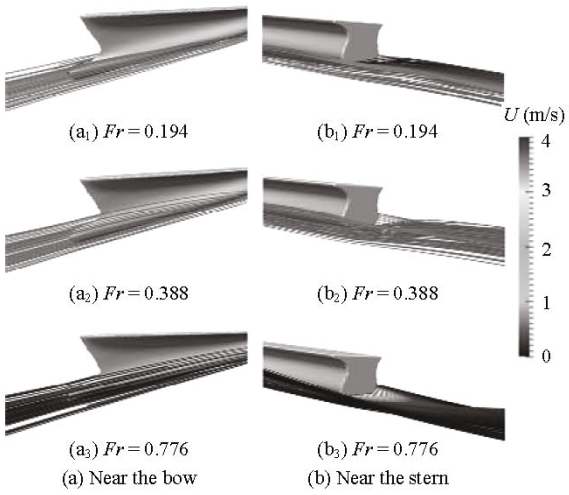

Fig.5 Streamlines near the bow and stern of one hull

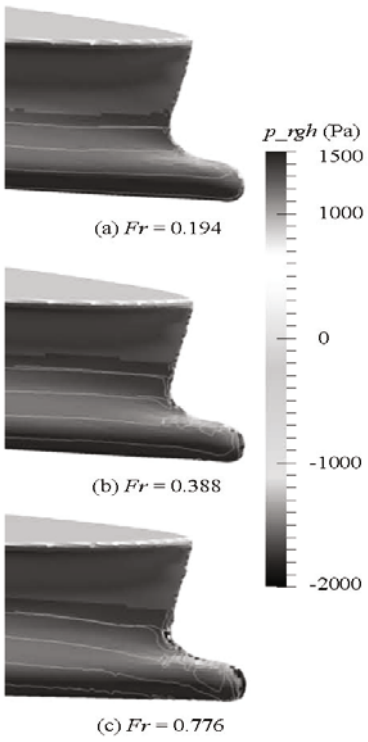

Fig.6 Pressure distribution around the bow

From Fig.5, the streamlines near the bow are smooth and regular. The intensity of bow wave is reduced by the bulbous bow. The homogeneous water particles flow into the bottom at aft end. In spite of the difference of flow velocity, neither bow waves nor obvious vortices are generated, providing a good performance of viscous pressure resistance. For the streamlines at the stern, wave trough and crest are generated with fluctuant streamlines. The increase of flow velocity enhances the level of chaos, which leads to a rise of pressure resistance. The streamlines distribution is symmetrical in the flow field for the other hull, in keeping the same with the analysis of free surface.

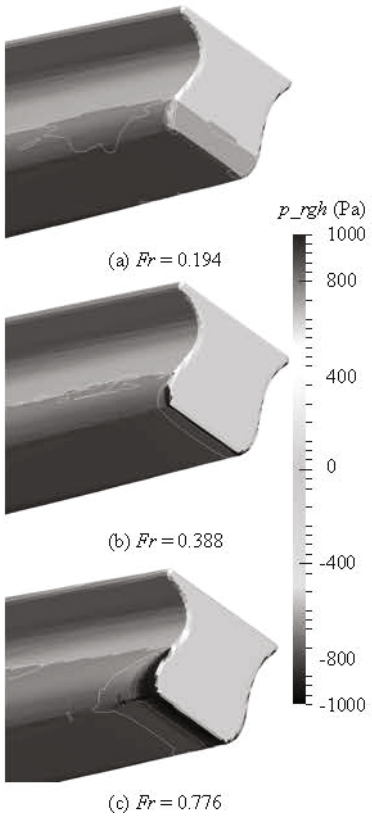

Fig.7 Pressure distribution around the stern

4.3 *Pressure distribution around the hull*

The pressure difference between bow and stern leads to viscous pressure resistance. The kinetic energy of water particle is dissipated by viscous effects. The pressure contour on the surface of hull affects the resistance performance as well. The pressure distribution under the water plane around the bow at different speed is shown in Fig.6. The pressure contour under the water plane around the stern at different speeds is shown in Fig.7.

For this catamaran, the peak value of pressure is concentrated on the end of bulbous bow. When the Froude number is as low as 0.194, no obvious peak points occur. The peak region expands and peak value increases with the increase of flow velocity. Moreover, higher pressure on stem post is found when the Froude number reaches 0.388 and 0.776, as shown in Fig.6. An obvious low pressure region is generated at the bottom of stern edge, as shown in Fig.7. On the contrary, the pressure of other parts on the hull surface is generally low. It reflects a larger pressure difference for the high velocity cases, which results in the higher viscous pressure resistance.

4.4 *Vorticity field near the hull*

The full simulation of the viscous flow field is studied by naoe-FOAM-SJTU in this paper. The generation of vortex would cause a severe pressure reduction and vibration of the hull. The simulation of vortices around the hull, especially between the twin hulls, is useful to evaluate the resistance and operation performance.

The X - direction vortices near the hull are shown in Fig.8. By slicing 15 transverse sections with the interval of 0.2 m, the vortices can be presented on sliced planes using the contour.

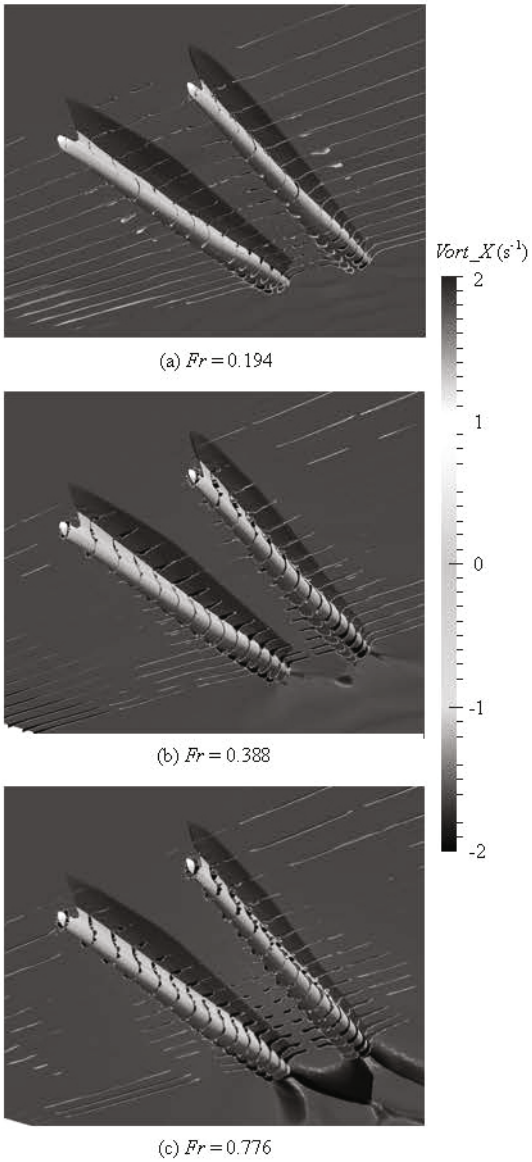

Fig.8 Vortices field around the catamaran hulls

Along with the increase of Froude number, the eddy structure can be observed more and more distinctly either on the hull surface or on the free surface. When the Froude number is 0.194, some small eddies begin to form. When the Froude number increases to 0.388, the eddy structure becomes chaotic and irregular. In addition, more eddies appear in the region between the two hulls. This phenomenon is more obvious for the Froude number of 0.776, which results from the interference of two hulls in the flow field. The pressure decrease is boosted by the eddies on the bilge and bottom of the catamaran. On the free surface, more vortexes are generated near the aft region of the twin hulls. In all, the vortex generation leads to a further increase on the viscous pressure resistance.

5. Conclusions

In this paper, numerical simulations focusing on a catamaran sailing in still water at different velocity conditions have been performed. A series of factors which affects the sailing performance have been considered. The study contains the calculation of resistance components, comparisons with the test data, free surfaces and wave-making simulations, the changes of vorticity field, analyses of pressure distribution and streamlines around the hull. Some meaningful conclusions can be summarized.

The RANS solver naoe-FOAM-SJTU is proved to be reliable to handle general fluid hydrodynamic issues with a good efficiency, which is the main purpose of the study in this paper. It has a good extendibility with high efficiency which will be able to solve more complex nonlinear problems in the future.

The resistance performances under different conditions of low, medium and high speed are studied respectively. With the increase of velocity, the change of flow field is becoming more and more severe. The results show that an outstanding resistance performance in high speed condition can be achieved. The computation data would be a good reference for future studies such as the design of catamran hull forms and arrangement.

As the future work, the solver naoe-FOAM-SJTU can be applied to the study of other hull forms. At a certain velocity, by the similar numerical simulations of different value of S_c / L_{pp} and other main dimensions, a catamaran with an optimum profile can be obtained. Moreover, for high speed conditions, the DOFs of hull body can be freed to consider about the effects of dynamic sinkage and trim. As the impressive computation efficiency and flexiablity, naoe-FOAM-SJTU would play a significant role in the field of viscosity hydrodynamic computation.

Acknowledgement

This work was supported by the High Technology of Marine Research Project of the Ministry of Industry and Information Technology of China, the Pro-

gram for Professor of Special Appointment (Eastern Scholar) at Shanghai Institutions of Higher Learning (Grant No. 2013022), and the Center for HPC of Shanghai Jiao Tong University, to which the authors are most grateful.

References

[1] SAHOO P. K., BROWNE N. A. and SALAS M. Experimental and CFD study of wave resistance of high-speed round bilge catamaran hull forms[C]. **Proceedings of 4th International Conference on High Performance Marine Vehicles.** Rome, Italy, 2004.

[2] CHEN Jing-pu, ZHU De-xiang and HE Shu-long. Research on numerical prediction method for wave making resistance of catamaran/trimaran[J]. **Journal of Ship Mechanics,** 2006, 10(2): 23-29(in Chinese).

[3] CASTIGLIONE T., STERN F. and BOVA S. et al. Numerical investigation of the seakeeping behavior of a catamaran advancing in regular head waves[J]. **Ocean Engineering**, 2011, 38(16): 1806-1822.

[4] CARRICA P. M., WILSON R. V. and STERN F. An unsteady single–phase level set method for viscous free surface flows[J]. **International Journal for Numerical Methods in Fluids,** 2007, 53(2): 229-256.

[5] DENG Rui, HUANG De-bo and YU Lei et al. Research on factors of a flow field affecting catamaran resistance calculation[J]. **Journal of Harbin Engineering University,** 2011, 32(2):141-147(in Chinese).

[6] JAMALUDDIN A., UTAMA I. and WIDODO B. et al. Experimental and numerical study of the resistance component interactions of catamarans[J]. **Proceedings of the Institution of Mechanical Engineers, Part M: Journal of Engineering for the Maritime Environment,** 2013, 227(1): 51-60.

[7] JASAK H. OpenFOAM: Open source CFD in research and industry[J]. **International Journal of Naval Architecture and Ocean Engineering,** 2009, 1(2): 89-94.

[8] ZHA Ruo-si, YE Hai-xuan and SHEN Zhi-rong et al. Numerical study of viscous wave-making resistance of ship navigation in still water[J]. **Journal of Marine Science and Application,** 2014, 13(2): 158-166.

[9] CHA Jing-jing, WAN De-cheng. Numerical wave generation and absorption based on OpenFOAM[J]. **The Ocean Engineering,** 2011, 29(3): 1-12(in Chinese).

[10] SHEN Zhi-rong, YE Hai-xuan and WAN De-cheng. Motion response and added resistance of ship in head waves based on RANS simulations[J]. **Chinese Journal of Hydrodynamics,** 2012, 27(6): 621-633(in Chinese).

[11] YE Hai-xuan, SHEN Zhi-rong and WAN De-cheng. Numerical prediction of added resistance and vertical ship motions in regular head waves[J]. **Journal of Marine Science and Application,** 2012, 11(4): 410-416.

[12] CAO Hong-jian, WAN De-cheng. Three-dimensional numerical wave tank based on naoe-FOAM-SJTU solver[J]. **Journal of Fudan University: Natural Science,** 2013, 52(5): 627-634.

[13] LIU Yuan-chuan, WAN De-cheng. Numerical simulation of motion response of an offshore observation platform in waves[J]. **Journal of Marine Science and Application,** 2013, 12(1): 89-97.

[14] SHEN Zhi-rong, WAN De-cheng. RANS computations of added resistance and motions of a ship in head waves[J]. **International Journal of Offshore and Polar Engineering,** 2013, 23(4): 263-271.

[15] DHAKAL T., WALTERS D. Curvature and rotation sensitive variants of the K-Omega SST turbulence model[C]. **ASME 2009 Fluids Engineering Division Summer Meeting.** USA, 2009.

[16] ZHAO Xi-zeng, HU Chang-hong and SUN Zhao-cheng. Numerical simulation of extreme wave generation using VOF method[J]. **Journal of Hydrodynamics,** 2010, 22(4): 466-477.

[17] HERVOUET J. M. **Hydrodynamics of free surface flows: Modelling with the finite element method**[M]. New York, USA: John Wiley and Sons, 2007.

[18] SEIF M. S., ASNAGHI A. and JAHANBAKHSH E. Implementation of PISO algorithm for simulating unsteady cavitating flows[J]. **Ocean Engineering,** 2010, 37(14): 1321-1336.